A Theoretical Study of the Meyer–Schuster Reaction Mechanism: Minimum-Energy Profile and Properties of Transition-State Structure

J. Andres,[†,⊥] R. Cardenas,[‡] E. Silla,[†] and O. Tapia*[‡]

Contribution from the Departamento de Quimica-Fisica, Universidad de Valencia, Burjasot (Valencia), Spain, and Department of Chemistry and Molecular Biology, BMC, Swedish University of Agricultural Sciences, Box 590, S-75124 Uppsala, Sweden.
Received March 2, 1987

Abstract: The rate-limiting step (RLS) in the mechanism proposed for the apparent 1,3-hydroxyl shift in α-acetylenic tertiary alcohols leading to α,β-unsaturated carbonyl compounds as final products has been studied with MINDO/3, CNDO/2, and ab initio analytical gradient procedures at restricted Hartree–Fock level. Three basis sets have been used: minimal (STO-3G) and two split valence shells (4-31G and 4-21G). The ability of the corresponding wave functions for describing the molecular mechanism and experimental information inferred on the transition-state structure is analyzed. CNDO/2 gives a completely unrealistic description. MINDO/3 produces a typical stepwise mechanism via an intermediate, but comparisons to available information disprove such a mechanism. The change to a minimal basis set representation did not improve agreement with mechanistic data. Double-ζ type basis set turns out to be the minimal level of representation yielding a picture that reproduces the information on solvent isotope effects and kinetic data. The 4-21G calculated transition-state structure corresponds to a slightly deformed alkynyl cation "solvated" by two water molecules. The mechanism corresponds to a concerted asynchronic process and may occur either as syn or anti attack with respect to the protonated hydroxyl group; both transition structures have nearly identical electronic properties. The 4-21G energy hypersurface has been further studied. Thus, along one perpendicular direction to the transition vector a second stationary point of critical index 2 is found which describes a solvated alkynyl cation. The appearance of this type of cation allows for a unified theoretical interpretation of the Meyer–Schuster reaction (2,3-hydroxyl shift) and Rupe reaction (1,2-hydroxyl shift). Information drawn from previous Monte Carlo simulations and the presence of the second stationary point of index 2 suggests the possibility of changing the saddle point into a carbonium ion intermediate by solvent caging effects. The driving force for both Meyer–Schuster and Rupe reaction rearrangements appears to be the irreversible process involved in the formation of unsaturated carbonyl compounds from the "intermediate" carbonium ions. The topography of the 4-21G energy hypersurface presents two solvation sites (minima of the hypersurface) for the protonated alcohol and two for the protonated allenol. The solvation minima of the protonated alcohol are connected via a saddle point whose structure is the reactant in the RLS. An analogous situation is found for the protonated allenol where the saddle point is now the product in the RLS. The protonated allenol and acetylenic alcohol solvated zones in the hypersurface are connected by the saddle point whose structure is the transition structure of the RLS. At the solvation saddles the orthogonal directions of the eigenvectors for the negative and the smallest positive eigenvalues of the force constant matrix are tangents to the pathway connecting the solvation sites to each other, and to the pathway connecting reactant and product in the RLS, respectively. This topography suggests that the Meyer–Schuster rearrangement is a solvent-assisted reaction. Monte Carlo simulations show that the solvation sites are occupied by solvent water molecules, and due to solvent caging effects, the reactant and product of the RLS in solution become stable species.

I. Introduction

A theoretical study of minimum-energy (ME) profiles and transition-state (TS) structures calculated for a molecular model that can undergo a Meyer–Schuster rearrangement is presented. This acid-catalyzed reaction describes a tertiary or secondary propargyl alcohol transposition to α,β-unsaturated carbonyl compounds (Scheme I).[1-3] The molecular mechanism proposed by Edens et al.,[1] which is based on kinetic and solvent isotope measurements, leads to a relatively well defined transition-state model. The mechanism consists of three steps. Oxygen protonation is the first (rapid) one. The second and rate-limiting step leads to an apparent 1,3-shift of the protonated hydroxyl group. The third describes a keto/enol tautomeric equilibrium followed by a rapid deprotonation. The TS structure and properties described in ref 1 set up a stringent test for gauging quantum chemical methods in their ability to produce reliable information in this respect. The present work addresses the rate-limiting-step (RLS) representation; emphasis is placed on determining the structure and electronic distribution of the TS with quantum chemical methods.

In the expected RLS two extreme situations, as a function of solvent constitution, can be distinguished: one corresponds to an anhydrous acid medium[2] and the other to an aqueous acid one.[1] In the former the protonated hydroxyl group must move from the C_1 center toward the C_3 center (Scheme II). Mechanistically, this can be done in two alternative ways: intramolecular versus

Scheme I

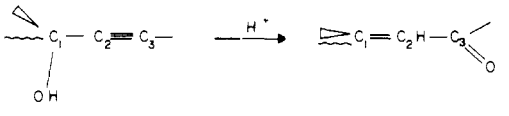

Scheme II

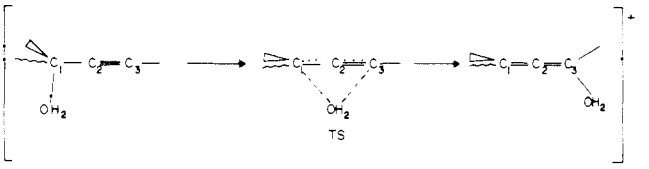

Scheme III

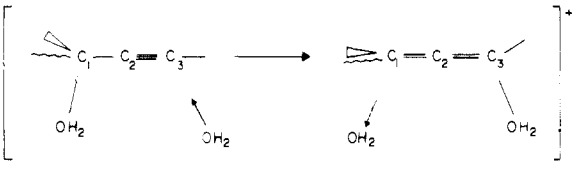

* Author to whom correspondence should be addressed.
† Universidad de Valencia.
‡ Swedish University of Agricultural Sciences.
⊥ Permanent address: Col. legi Universitari Castello.

(1) Edens, M.; Boerner, D.; Chase, C. R.; Nass, D.; Schiavelli, M. D. *J. Org. Chem.* **1977**, *42*, 3403.
(2) Swaminathan, S.; Narayan, K. V. *Chem. Rev.* **1971**, *71*, 429.

0002-7863/88/1510-0666$01.50/0

solvolytic transposition. Analytical gradient studies[4,5] with both semiempirical (CNDO/2 and MINDO/3) and ab initio (STO-3G and 4-31G basis set level) molecular orbital methods have shown a transition state involving an alkynyl cation[5]

$$[R^1R^2C_1 \cdots C_2 \equiv C_3R^3]^+$$

interacting, electrostatically, with a water molecule resulting from the protonated hydroxyl group. This structure corresponds better with the solvolytic mechanism and it agrees with the experimental detection of alkynyl cations in hyperacid (anhydrous) media.[6] However, for aqueous acid media this model is not adequate since the probability of finding a solvent water molecule in the neighborhood of C_3 is high enough[7] to warrant Edens' et al.[1] intermolecular mechanism[8] (Scheme III). The putative TS structure requires a water molecule coming from the solvation shell which will attack the C_3 center. The more simple model to represent the solvent is an ancillary water molecule interacting with the protonated alcohol: the minimal solvation model. In this work we will focus on this minimal solvated model (MSM) to describe the apparent 1,3-hydroxyl shift in the RLS. The basic molecular model $R^1 = R^2 = CH_3$ and $R^3 = H$ corresponds to a molecule capable of supporting the chemical reaction.

The energy hypersurface is a basic tool for building a dynamic description of a particular chemical reaction.[9] First principle quantum chemical calculations of hypersurfaces for realistic model systems are beyond present computer capabilities. However, for most chemical systems in solution the theoretical analysis and correlation with kinetic data is done either in the framework of the transition-state theory[10-13] or in Kramer's theory of activated processes.[13-15] Thus, an appropriate minimum energy (ME) profile may suffice to locate these stationary points for the RLS. For relatively small molecular systems high-quality atomic basis sets have been used to determine reactive ME profiles.[16] However, as the size of the molecular system increases, either the quality of the basis set has to be downgraded or semiempirical MO methods must be employed. Among these latter methods, MINDO/3 has been used extensively to study reaction mechanisms.[17] Together with other important approximate MO methods they have been used to study S_N2, S_N2', and other multibond reactions[17b] that have some similarities with the present one. In view of the large number of geometric parameters to be optimized (36 for the tertiary alcohol, 48 for the MSM) MINDO/3 and CNDO/2 MO methods have been used to study an ME profile describing the RLS. Stationary points on the corresponding energy hypersurfaces are calculated in order to determine the properties of reactant, product, and intermediate(s) (if any) and the nature of the TS(s) for the MSM. The ME profiles obtained with these methods conflict with each other and available information on the mechanism and kinetics. This situation prompted a STO-3G basis set calculation of the same ME profile. A careful confrontation between theoretical results and the mechanistic information at our disposal[1] shows even more serious clashes than MINDO/3. Unfortunately, this does not provide evidence in favor of MINDO/3 reliability.

An important objective of the present work is to find a theoretical framework for describing the TS properties as they are inferred from experimental probes. The failure of the STO-3G basis set to render an adequate description of the TS can be overcome by using double-ζ type basis set. This increases the computational burden to critical levels if both split valence shell basis sets and realistic molecular model systems have to be studied. Therefore, attention is focused first on stationary points of the energy hypersurface. For realistic molecular systems the most difficult is the saddle point location since the calculation of minima is considered as routine work.[18] The saddle point will be bracketed by using a simple strategy based on ME profiles obtained from less expensive MO methods.[19]

The saddle point region for either 4-21G or 4-31G basis sets is explored from the STO-3G TS geometry (TS(STO-3G)). As previously noticed (cf. intramolecular mechanism (Scheme II) in ref 19) this procedure helps find the exact stationary point. The 4-21G//STO-3G and 4-31G//STO-3G basis set calculations showed a trend of the charge distribution which goes in the correct direction pointed by the experimental information.[1] This outcome prompted the determination of the fully optimized saddle point with the 4-21G basis set. The stationary point has been characterized by calculating the relevant force constants. The corresponding TS structure provides a description agreeing with the information concerning the physical chemistry of this reaction.

In the RLS there are two channels leading to the same final result: one is the syn-attack of the incoming water molecule as depicted in Scheme III; the other corresponds to the anti-sttack. The stationary point geometries for the RLS of the anti-form are obtained from the syn-form after changing the dihedral angles of the atoms making a bond to C_3. The electronic structure of both TSs is otherwise identical.

The MSM is a first step toward representing solvent effects on a reaction mechanism. Besides the stationary points describing the RLS, the 4-21G energy hypersurface topography presents local solvation sites (e.g., protonated alcohol fragment and acetylenic carbo acid). They appear as minima connected by a continuous pathway (geodesic) passing through the reactant of the RLS discussed above. Along this solvation geodesic the reactant in the RLS is a maximum, thereby transforming the reactant in a saddle point of the global hypersurface. A similar situation is found when the reaction proceeds from the protonated allenol. Thus, the representation of the rate-limiting step on the 4-21G hypersurface consists of a reaction geodesic connecting three saddle points. One of the differences in interpreting a model energy surface for a reaction in vacuo and in condensed phase emerges here. The solvation sites in the aqueous liquid phase are bound to be occupied by solvent water molecules. This result follows from analysis of the Monte Carlo simulations.[7] The reactant and product of the RLS become stabilized by solvent caging effects. Since the TS for the RLS calculated here adequately represents many of the physical chemistry properties, one would expect this TS to be

(3) Olsson, L. I.; Claesson, A.; Bogentoft, C. *Acta Chem. Scand.* **1973**, *27*, 1629.
(4) Andres, J.; Arnau, A.; Silla, E.; Bertran, J.; Tapia, O. *J. Mol. Struct. THEOCHEM.* **1983**, *105*, 49.
(5) Andres, J.; Silla, E.; Tapia, O. *J. Mol. Struct. THEOCHEM.* **1986**, *138*, 171.
(6) (a) Olah, G. A.; Spear, R. J.; Waterman, P. W.; Denis, J. M. *J. Am. Chem. Soc.* **1974**, *96*, 5855. (b) Hanack, M. *Acc. Chem. Res.* **1976**, *9*, 371.
(7) Tapia, O.; Lluch, J. M. *J. Chem. Phys.* **1985**, *83*, 3970.
(8) Andres, J.; Silla, E.; Tapia, O. *Chem. Phys. Lett.* **1983**, *94*, 193.
(9) (a) Pechukas, P. *J. Chem. Phys.* **1976**, *64*, 1516. (b) Tachibana, A.; Fukui, K. *Theor. Chim. Acta* **1978**, *49*, 321; **1979**, *51*, 189; **1980**, *57*, 81. (c) Mezey, P. G. *Theor. Chim. Acta* **1980**, *54*, 95; **1981**, *58*, 309; **1981**, *60*, 97; **1982**, *60*, 409; **1982**, *62*, 133. (d) Muller, K. *Angew. Chem., Int. Ed. Engl.* **1980**, *19*, 1. (e) Scharfenberg, P. *Theor. Chim. Acta* **1979**, *53*, 279; **1980**, *58*, 73; *Chem. Phys. Lett.* **1981**, *79*, 115; *J. Comput. Chem.* **1982**, *3*, 277. (f) Morokuma, K.; Sato, S.; Kitaura, K.; Obara, S.; Ohta, K.; Hanamura, M. *New Horizons of Quantum Chemistry*; Lowdin, P. O., Pullman, B., Eds.; Reidel: Dordrecht, 1983. (g) Salem, L. *Electrons in Chemical Reactions*; Wiley-Interscience: New York, 1982. (h) Schegel, H. B. *J. Comput. Chem.* **1984**, *3*, 214. (i) Miller, W. H. *J. Phys. Chem.* **1983**, *87*, 3811. (j) Havlas, Z.; Zahradnik, R. *Int. J. Quantum Chem.* **1984**, *26*, 607.
(10) (a) Glasstone, S.; Laidler, K. J.; Eyring, H. *The Theory of Rate Processes*; McGraw-Hill: New York, 1941. (b) Laidler, K. J. *Theories of Chemical Reaction Rates*; McGraw-Hill: New York, 1969. (c) Laidler, K. J.; King, M. C. *J. Phys. Chem.* **1983**, *87*, 2657.
(11) Chandler, D. *J. Chem. Phys.* **1978**, *68*, 2959.
(12) (a) Truhlar, D. G.; Garrett, B. C. *Acc. Chem. Res.* **1980**, *13*, 440. (b) Garrett, B. C.; Truhlar, D. G. *J. Am. Chem. Soc.* **1980**, *102*, 2559. (c) Truhlar, D. G.; Hase, W. L.; Hynes, J. T. *J. Phys. Chem.* **1983**, *87*, 2664.
(13) (a) Northrup, S. H.; Hynes, J. T. *J. Chem. Phys.* **1980**, *73*, 2700. (b) Grote, R. F.; Hynes, J. T. *J. Chem. Phys.* **1980**, *73*, 2715; **1981**, *75*, 2191. (c) Van der Zwan, G.; Hynes, J. T. *J. Chem. Phys.* **1982**, *76*, 2993; **1983**, *78*, 4174. (d) Hynes, J. T. In *Theory of Chemical Reactions*; Bard, M., Ed.; CRC Press: FL, 1986. (e) Hynes, J. T. *Annu. Rev. Phys. Chem.* **1985**, *36*, 573.
(14) (a) Kramers, H. A. *Physica* **1940**, *7*, 284. (b) Chandrasekhar, S. *Rev. Mod. Phys.* **1943**, *15*, 1.
(15) Adelman, S. A. *J. Chem. Phys.* **1984**, *81*, 2776.
(16) Jug, K. *Theor. Chim. Acta* **1980**, *54*, 263.
(17) (a) Lewis, D. F. V. *Chem. Rev.* **1986**, *86*, 1111 and references therein. (b) Dewar, M. J. S. *J. Am. Chem. Soc.* **1984**, *106*, 209.
(18) Schafer, L. *J. Mol. Struct. THEOCHEM* **1983**, *100*, 1.
(19) Tapia, O.; Andres, J. *Chem. Phys. Lett.* **1984**, *109*, 471.

poorly solvated, thereby conserving the geometric and electronic structural features that make it a portrait of the TS proposed by Edens et al.[1]

In section II the molecular models and computational schemes are described. The ME profiles describing the RLS for the model molecule are discussed in section III. The TS structure and properties are analyzed in section IV. In section V the theoretical results are contrasted against the experimental information on the TS at disposal. A general discussion is presented in the last section.

II. Models and Computational Schemes

The molecular model used to carry out the computing is the oxygen-protonated α-acetylenic alcohol $[(CH_3)_2C(OH_2)C{\equiv}CH]^+$ plus one solvent water molecule. It is well established that the 1,3-hydroxyl shift is usually accompanied by a 1,2-hydroxyl shift in the same compounds (Rupe reaction). An alkynyl cation plays a central role in the mechanism of these reactions.[1-3,20,21] In this paper we will discuss the 1,3-hydroxyl shift; however, the results obtained help in the understanding of the relationships between both. The molecular model selected here is the smallest one can build that can undergo both rearrangements.

The approximate MO SCF calculations have been carried out with the GEOMO program[22] including Rinaldi's gradient optimization routines.[23] CNDO/2[24] and MINDO/3[25] approximate MO schemes have been used. The optimizations were terminated after the average gradient length was less than 10^{-6} atomic units. The transition states in MINDO/3 calculations have been localized by using the programs SIGMA and FORCE.[26]

The ab initio calculations have been performed with the MONSTERGAUSS program.[27,28] The computations were carried out at both minimal (STO-3G)[29] and split valence shell 4-21G[30] and 4-31G[31] basis set level in the restricted Hartree–Fock formalism.[32] Analytical gradients[33] of the SCF HF energy with respect to the internal geometric parameters have been used. The optimally conditioned minimization technique[34] has been used to calculate the ME profiles. Actually, the nature of this technique only ensures zero-gradient condition along all coordinates except the one used as a constraint. The stationary points have been located with the VA05 subroutine,[35] and the index has been determined by diagonalizing the force constant matrix. The calculation of the Hessian matrix by finite differences is extremely CPU-time demanding. For this reason a one-sided-step method was used to calculate them from the force.

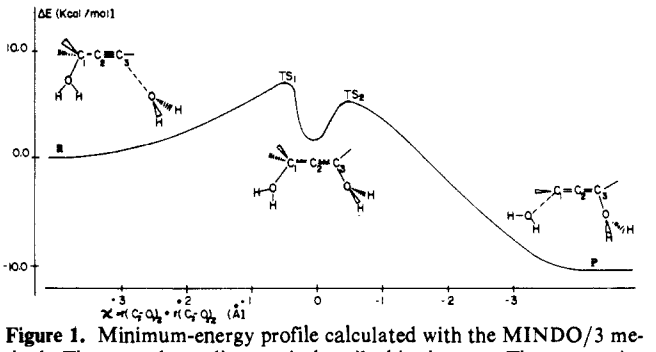

Figure 1. Minimum-energy profile calculated with the MINDO/3 method. The control coordinate χ is described in the text. The geometries of the TS_1 and TS_2 are described in Figure 3.

In the procedure used to obtain the transition-state structure the internal coordinate space is partitioned into two subspaces.[19] One is the control space including all internal degrees of freedom, the force constant of which changes as the reaction progresses. The set of internal coordinates that are subsidiarily changed as the reaction proceeds is defined as complementary space. This means that a partitioning of the force constant matrix into two weakly interacting subspaces is possible. In the present case the control space includes the internal coordinates of the alkynyl fragment, the two water fragments, and the bond dihedral angles defining the methyl carbons (symmetric combination).

In practice, the approximate MO and STO-3G calculations are carried out with one-parameter constraint chosen in the control space. All remaining parameters in the control space are optimized with the fast optimally conjugated gradient method.[34] The plot of energy as a function of the constraint parameter is not always adequate in getting a continuous profile.[9d] A better procedure is to plot the energy as a function of a one-dimensional coordinate (the control coordinate χ) whose variation reflects the important geometrical changes as the system goes continuously from the reactant to the products via the TS.[19] In the present case the control coordinate χ is the projection along the z-axis, which coincides with the C_1–C_2 direction, of the vector position of oxygen atoms, $\vec{r}(C_2\text{–}O_1)_z + \vec{r}(C_2\text{–}O_2)_z$; the origin of the reference frame is centered at C_2. Other choices are possible but they do not change the results. With the computational procedures used in this work, the stationary points on the energy profile $E(\chi)$ are also stationary points on the global energy hypersurface. This type of profile is referred to as minimum energy profile in what follows. The χ coordinate ranges from ca. -4 to $+4$ Å in semiempirical calculations; the range is somewhat smaller in ab initio calculations.

The optimizations have been terminated after the gradient length of the unconstrained parameters (control space) is reduced to below 5×10^{-2} mdyn or mdyn Å/rad. The overall average gradient length is less than 5×10^{-4} mdyn or mdyn Å/rad. The second derivatives for the maximum in this minimum energy profile are calculated in the control space and the corresponding matrix diagonalized.

Charge-transfer effects are calculated with the help of Mulliken's population analysis.[36] Otto and Ladik[37] have shown that this method gives a qualitatively correct description of the charge-transfer process.

III. ME Profiles

The model suggested in ref 1 leads to a simple pathway for the RLS: a nucleophilic attack of one water molecule at C_3 (Scheme III). Quantum chemical studies[38] show that the energy depends weakly on the oxygen dihedral angle of the water molecule. The potential energy profile is shallow and presents minima at both cis and trans configurations. Note that Monte Carlo simulations[7] on the reactant of this reaction show water molecules that can attack C_3 both in anti and syn positions. The attack may be syn

(20) (a) Chaudhuri, N. K.; Gut, M. *J. Am. Chem Soc.* **1965**, *87*, 3737. (b) Apparu, M.; Glenat, R. *Bull. Soc. Chim. Fr.* **1968**, 1106, 1113.
(21) Vartanyan, S. A.; Babayan, S. O. *Russ. Chem. Rev.* **1967**, *36*, 670.
(22) Rinaldi, D. *QCPE* **1975**, *11*, 290.
(23) Rinaldi, D. *Comput. Chem.* **1976**, *1*, 109.
(24) Pople, J. A.; Segal, G. A. *J. Chem. Phys.* **1966**, *44*, 3289.
(25) Bingham, R.; Dewar, M. J. S.; Lo, D. H. *J. Am. Chem. Soc.* **1975**, *97*, 1285.
(26) SIGMA program which locates stationary points through the minimization of the square of the gradient norm and FORCE program which determines its nature by calculating the eigenvalues of the force constant matrix.
(27) Peterson, M. R.; Poirier, R. A. Program MONSTERGAUSS, University of Toronto, Ontario, Canada 1980. In addition to the GAUSSIAN 70 integral and SCF routines,[28] the program incorporates analytical gradients and automatic optimizations with or without constraints.
(28) GAUSSIAN 70: Hehre, W. J.; Lathan, W. A.; Ditchfield, R.; Newton, M. D.; Pople, J. A. *QCPE* No. 236.
(29) Ditchfield, R.; Stewart, R. F.; Pople, J. A. *J. Chem. Phys.* **1969**, *51*, 2657.
(30) Pulay, P.; Fogarasi, G.; Pang, F.; Boggs, J. E. *J. Am. Chem. Soc.* **1979**, *101*, 2550.
(31) Ditchfield, R.; Hehre, W. J.; Pople, J. A. *J. Chem. Phys.* **1971**, *54*, 724.
(32) Roothaan, C. C. J. *Rev. Mod. Phys.* **1951**, *23*, 69.
(33) Schlegel, H. B. program Force, Ph.D. Thesis, Queen's University, Kingston, Ontario, Canada, 1975.
(34) (a) Davidson, N. C. *Math. Prog.* **1975**, *9*, 1. (b) Bell, S.; Crighton, J.; Fletcher, R. *Chem. Phys. Lett.* **1981**, *82*, 122.
(35) Powell, M. J. D. VA05 program, Harwell Subroutine Library. Atomic Energy Research Establishment, Harwell, U.K.
(36) Mayer, I. *Chem. Phys. Lett.* **1983**, *97*, 270.
(37) Otto, P.; Ladik, J. *Int. J. Quantum Chem.* **1980**, *18*, 1143.
(38) Andres, J. Ph.D. Thesis, University of Valencia, Spain, 1983.

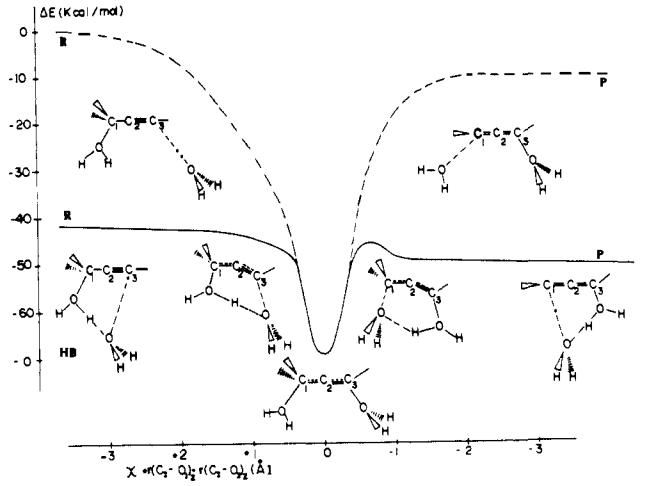

Figure 2. CNDO/2 ME profile; the dashed line describes Edens' pathway. In this hypersurface there is a minimum of lower energy than Edens' arrangement where the incoming water makes an H bond with the protonated hydroxyl group (plain line). (MINDO/3 cannot detect this interaction.[69]) On the negative χ region a symmetry plane element is conserved. On the positive side of χ the pictures describing the typical structures show a loss of local symmetry that may be the reason for the maximum according to the theorem by Stanton and McIver;[39,70] this profile is not adequate in representing the system in a condensed phase as the water cannot move upwards freely.

or anti with respect to the protonated alcohol fragment as there is no stereospecificity associated with the C_3 center; here the cis arrangement is used for discussions. The C_3–O_2 distance (R_1) is used as a constraint; all the remaining variables in the control space are geometrically optimized, in particular $R_2 = C_1$–O_1. The overall gradient length is somewhat better than the threshold used in the control space since the coordinates in the complementary space are much more relaxed. The energy is plotted as a function of the control coordinate χ, which must be calculated with the optimized geometry at each point. The χ coordinate serves to handle correctly the available information.

The ME profiles calculated with MINDO/3 and CNDO/2 procedures for the RLS described in Scheme III are reported in Figures 1 and 2, respectively. The geometric structures characteristic of each region along these curves are also depicted.

The ME profile must describe a process where a bond is formed and another is broken along R_1 and R_2 coordinates. While the semiempirical calculations do describe the overall feature, the profiles are totally different. At the region around $\chi = 0$ in both calculations there is a mimimum at that position: the eigenvalues of the Hessian are all positive. MINDO/3 describes a metastable state, while CNDO/2 displays an absolute minimum. The geometry at this point in both calculations is similar. Judging from the interatomic distances, R_1 = 1.55 and 1.49 Å and R_2 = 1.48 and 1.45 Å for MINDO/3 and CNDO/2, respectively, both interactions appear to be strong or, in ref 1 language they have a covalent-like nature rather than electrostatic. Furthermore, there is a sizable charge transfer from the water fragments toward the alkynyl frame (0.46 and 0.74 au of charge for MINDO/3 and CNDO/2, respectively).

The MINDO/3 profile has two saddle points TS_1 and TS_2 (cf. Figure 1). The geometric structure of TS_1 corresponds to a "covalent-like" bond for R_2 (1.49 Å) and an electrostatic-like interaction for R_1 (1.96 Å) (see Figure 3). The activation energy ($E_{TS_1} - E_R$) amounts to 6.7 kcal/mol. The transition vector[39] is associated to R_1 distance, and the amplitude on the R_2 distance is negligible. The intermediate is 1.35 kcal/mol above the reactant. The geometry of TS_2 corresponds to an electrostatic-like interaction between C_1 and O_1 (R_2 distance 1.87 Å) and covalent for R_1 (distance 1.44 Å, see Figure 3). The energy height from the intermediate to TS_2 is 3.7 kcal/mol. The transition vector now

(39) McIver, J. W., Jr. *Acc. Chem. Res.* **1974**, *7*, 72.

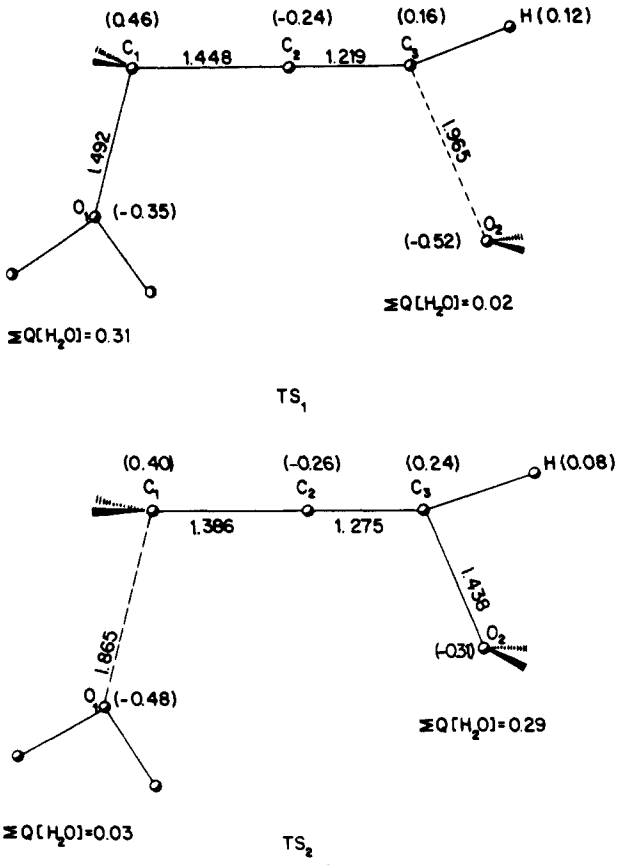

Figure 3. Transition-state structures calculated with the MINDO/3 (TS_1 and TS_2). Stationary distances (Å) and net atomic charges (in parentheses) are drawn. The angle $\angle C_2C_3H$ is for TS_1 = 163.79° and TS_2 = 136.86°. (The rehybridization change at C_3 can be measured by this angle.)

is dominated by the amplitude at R_2, and the R_1 amplitude is negligible. Mechanistically, this ME profile describes a two-step reaction via a stable intermediate, where the first step is rate determining.

The CNDO/2 ME profile is in total disagreement with the tenets of the intermolecular mechanism proposed on experimental grounds. It fails to produce a barrier for this reaction. CNDO/2 and INDO (calculations not reported[38]) are totally unreliable in representing the RLS of the 1,3-hydroxyl shift.

The MINDO/3 ME profile has some weak points: TS_1 has a too large covalent interaction along the C_1–O_1 distance. Furthermore, nowhere on this profile is an alkynyl-like cation obtained, which is one of the key elements in the mechanistic description of both the Meyer–Schuster and Rupe reactions.[1-3,20,21] This failure might be due to the weaknesses of this method in representing regions where bonds are forming and breaking. However, the possibility that the calculations do not reproduce an alkynyl-like cation due to the exclusion of solvation effects cannot be ruled out.

The ME profile obtained with a STO-3G basis set in the intermolecular mechanism is depicted in Figure 4: the R–TS–P curve. This profile presents the maximum at TS that corresponds to a saddle point on the energy hypersurface. An energy barrier of 24.4 kcal/mol is found that is larger than the first activation energy (TS_1) in the MINDO/3 profile (6.7 kcal/mol). The geometry of the TS(STO-3G) (the C_1–O_1 and C_3–O_2 distances are 1.77 and 1.65 Å, respectively) differs from the one found with MINDO/3.[8]

The mechanistic probes used in ref 1 lead to an ion–dipole model at the reaction center C_1 and a partially "covalent" state at the rearrangement center C_3. This description emphasizes the fact that the interaction strengths at the C_1 and C_3 centers must be different, and in particular the interaction strength at C_3 is larger than that at C_1. This effect can be sensed by solvent isotope effects

Table I. Data Concerning the Saddle Point Obtained in Different Basis Sets[a]

	internal coordinates	STO-3G//STO-3G $\epsilon^b = -1.568$			4-31G//STO-3G $\epsilon^b = -1.019$			4-21G//STO-3G $\epsilon^b = -0.866$			4-21G//4-21G $\epsilon^b = -0.307$		
		C^c	G^d	F^e	C	G	F	C	G	F	C	G	F
1	$\rho_{C_1-C_2}{}^f$	0.238	0.001	8.8	0.214	0.112	6.6	0.225	0.105	6.8	0.103	−0.045	7.6
2	$\rho_{C_2-C_3}$	−0.187	0.008	18.0	−0.153	0.101	16.5	−0.154	0.092	16.8	−0.079	0.023	16.7
3	$\rho_{C_3-O_2}$	0.549	−0.008	2.1	0.543	−0.295	1.9	0.545	−0.238	2.0	0.514	−0.018	0.7
4	$\rho_{C_1-O_1}$	−0.627	0.000	3.2	−0.644	−0.294	1.7	−0.627	−0.227	1.9	−0.649	−0.003	0.7
5	$\angle C_1C_2C_3$	−0.095	0.002	1.6	−0.091	−0.025	1.6	−0.079	0.017	1.6	−0.033	0.001	1.5
6	$\angle HC_3C_2$	0.265	0.006	1.4	0.353	−0.020	1.1	0.367	−0.012	1.1	0.408	−0.013	0.7
7	$\angle O_2C_3C_2$	−0.171	−0.003	2.1	−0.124	−0.059	1.7	−0.124	−0.004	1.7	−0.058	0.002	0.8
8	$\angle O_1C_1C_2$	−0.127	−0.001	2.3	−0.124	−0.059	2.0	−0.132	−0.003	2.0	−0.347	0.041	1.1
9	$\angle C_{met}C_1C_2{}^g$	−0.106	0.000	5.1	−0.102	0.002	4.8	−0.108	0.008	5.0	−0.004	0.021	5.2
10	$w(C_{met})^g$	0.277	0.000	3.8	0.218	−0.017	3.6	0.224	0.016	3.7	0.083	0.014	3.5

[a] The eigenvector coefficients (C) corresponding to the unique negative eigenvalue of the force constant matrix in the control subspace are reported together with the associated gradients (G) and the diagonal force constant (F). The calculations with the split valence shell basis set were further optimized with two iterations in the VA05 subroutine. The geometry of the STO-3G TS has been published in ref 8. [b] Unique negative eigenvalue of force constant matrix in mdyn/Å. [c] Components of eigenvector (transition vector) of force constant matrix. [d] Gradient in mdyn or mdyn Å/radian. [e] Second derivative of the total energy (force constant) with respect to internal coordinates. [f] ρ = distance (Å), $\angle$ = angle (deg), w = dihedral (deg). [g] Symmetric combination.

Table II. Bond Order (BO) and Exchange Component (E_{AB} in au) to the Leading Interatomic Electrostatic Term as Defined by Mayer[36] for Indicated Atom Pairs in Control Space[a]

	STO-3G//STO-3G			4-31G//STO-3G		4-2G//STO-3G		4-21G//4-21G		
R	P (Å)	BO	E_{AB}	BO	E_{AB}	BO	E_{AB}	P (Å)	BO	E_{AB}
$\rho_{C_1-C_2}$	1.389	1.4050	1.0708	1.2118	0.9236	1.2038	0.9174	1.339	1.3372	1.0569
$\rho_{C_2-C_3}$	1.222	2.2324	1.9336	2.5615	2.2186	2.4214	2.0973	1.215	2.5179	2.1927
$\rho_{C_3-O_2}$	1.743	0.4236	0.2572	0.1646	0.0999	0.2347	0.1425	2.162	0.1181	0.0578
$\rho_{C_1-O_1}$	1.764	0.3022	0.1813	0.1667	0.1000	0.2136	0.1281	2.638	0.0281	0.0128
$\sum E_{AB}$			3.4429		3.3422		3.2854			3.3186
$\sum E_{CO}$			0.4385		0.2000		0.2706		0.0691	

[a] The sum total $\sum E_{CO}$ and the sum over the C_1–O_1 and C_3–O_2 atom pairs are given. d (Å) is the equilibrium interatomic distance calculated with the basis set indicated in the head line.

(k_{H_2O}/k_{D_2O}), and the degree of hybridization at the C_3 center can be guessed from the inverse α-secondary isotope effect (k_H/k_D) observed.[1] Very little charge transfer (if any) from the water fragments toward the alkynyl frame can be inferred from these data.

Although the topology of the TS(STO-3G) agrees with the MSM, the geometry is too tight, i.e., the interatomic distances R_1 and R_2 are too short thereby leading to a large charge transfer (+0.31 and +0.23 unit of positive charge on the water fragments, respectively). This charge transfer is much too large to be compatible with available information.[1-3,20,21] Moreover, the TS obtained with STO-3G produces a much too large rehybridization at C_3 (see section V for discussion).

It is most likely that the charge-transfer effect is due to the nature of the basis set because 4-31G//STO-3G and 4-21G//STO-3G calculations at the TS point display a significantly smaller charge transfer (+0.15 and +0.16 in the former case, and +0.19 and +0.18 for the latter). It is apparent that the intermediate region of the energy hypersurface around the TS, where partial bonds are present, is difficult to represent either with semiempirical or minimal basis set methods. The use of these methods is usually justified in view of the large number of geometric parameters to be optimized. However, in the present case the results are not satisfactory, and the effort of increasing the complexity level of the basis set cannot be avoided. The next step is to study the system with basis set at a double-ζ level. In principle, this type of basis set should describe the intermediate distance region for R_1 and R_2 in the TS in a better way than in the minimal basis set.

IV. Transition-State Properties

(1) Basis Set Dependence. To check basis set effects, the geometry of the TS(STO-3G) has been used to calculate the electronic structure and second-order derivative of the total energy (which will be referred to, somewhat improperly, as force constants) with both 4-31G and 4-21G basis sets. In Table I we present the eigenvector, force constant, and gradient for all the variables in the control space corresponding to the unique negative eigenvalue of the force constant matrix.

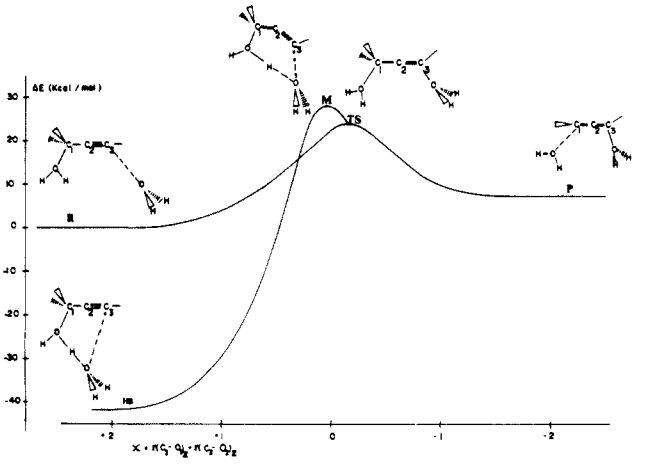

Figure 4. STO-3G ME profile; the R–TS–P line describes Edens' pathway; the HB–M–TS–P profile is a result of the constraint introduced. Note that the situation at M is not the one described by the Murrell–Laidler theorem[71] since the maximum is not a hilltop. Here there is a non-nihl gradient in a direction orthogonal to the control coordinate (basically the symmetric combination of the C_1–O_1 and C_3–O_2 distances). In view of ref 51 this is only a computational artifact.

A first result concerns the invariance of the number of negative eigenvalues as well as the transition vector to a change in basis set (cf. Table I). The relative weights of the transition vector components are roughly the same and the signs are retained. Thus, for all of them, the antisymmetric combination of R_1 and R_2 is the dominant feature.

The change of each gradient component in the control space is relatively small, except for the variables suffering dissociation, i.e., R_1 and R_2. The sign of the gradient is always negative, indicating that these distances should be elongated by relaxing to the stationary point. (The 4-21G//STO-3G and 4-31G//STO-3G points on the energy hypersurfaces are no longer stationary.) The bond order index and the non-classical exchange contribution to the leading interatomic electrostatic term[36] reflect

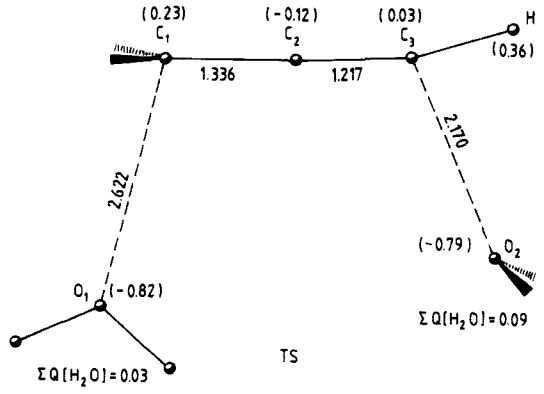

Figure 5. Saddle point corresponding to the TS in the MSM (syn attack) calculated with the 4-21G basis set. The geometric information of the 4-21G transition state is as follows: C_3–H = 1.058 Å, $\angle C_1C_2C_3$ = 178.16°, $\angle O_2C_3C_2$ = 110.57°, $\angle O_1C_1C_2$ = 104.20°; methyl group $C_{met}C_1$ = 1.520 Å, $\angle C_{met}C_1C_2$ = 120.34°, C_{met}–H = 1.080 Å, $\angle HC_{met}C_1$ = 110.34°, dihedral angle $C_{met}C_1C_2D$ = 86.05° where D is a dummy atom on top of C_2 and in the sheet plane. The dihedral angles defining the methyl hydrogens are 60°, –60°, and 180°; left water (O_1) O–H = 0.967 and 0.964 Å, ∠HOH = 113.19°, right water (O_2) O–H = 0.966 Å, ∠HOH = 111.21°, dihedral $HO_2C_3C_2$ = 106.82°. The angle $\angle C_2C_3H$ is 165.42°. The saddle point for the anti attack is obtained by changing the dihedral angle of the atoms bound to C_3.

in a similar way as the gradient the change of basis set. In Table II these indices are summarized for the interatomic distances of interest in the control space. A glance at this table shows that the minimal basis set overestimates this type of exchange forces only for the variables R_1 and R_2, while standard bonds are changed marginally.

The behavior of the internal coordinates included in the control space can be gathered into two subgroups: (1) the variables R_1 and R_2 defining the entering and exiting groups, and (2) the remaining coordinates in the control space which involve relatively standard chemically bound atoms (e.g., C_1–C_2, C_2–C_3). Thus, whenever a standard bonding situation is met, STO-3G calculations lead to relatively good estimates of equilibrium distance. It fails at the TS region where drastic changes in the bonding pattern are taking place. Interestingly, the geometry of the TS(STO-3G) is a point lying in the quadratic region around the actual saddle point on the 4-31G and 4-21G hypersurfaces. This fact shows that when geometries of possible intermediates, similar to the one obtained with MINDO/3, are used with these basis sets no stationary points are found. Starting from such geometries, and descending along the direction of symmetric combination of R_1 and R_2 ($R_1 - R_2$ constant), convergency is rapidly attained toward the actual saddle point.

(2) 4-21G Transition-State Structure. The saddle point with the 4-21G basis set has been determined by using the method described in ref 19 and also as a walk down along the $R_1 + R_2$ direction as indicated above. These procedures converge to the same point. The results concerning the geometry and other molecular indices are summarized in Figure 5 and Table I.

As expected from the gradients of 4-21G//STO-3G calculation, changes from the STO-3G geometry[8] are not negligible only for the oxygen–carbon distances. The coordinates C_1–O_1 and C_3–O_2 increase by 0.85 and 0.52 Å, respectively. Otherwise, the change of basis set marginally affects typical bond distances; the alkynyl structure shrinks a little (the distance C_1–C_3 is shortened). Nevertheless, the total energy decreases by ca. 18 kcal/mol as the geometry relaxes from the initial point.

The absolute value of the unique negative eigenvalue decreases when the basis set is upgraded. The relative signs of the component of the transition vector are conserved (cf. Table I). The antisymmetric combination of R_1 and R_2 dominates the transition vector.

The force constants for both TS structures (4-21G and STO-3G) cluster into two classes. Those associated with relatively normal chemical bonds are fairly invariant, while those dominating the control coordinate are sensitive to the change in basis set. In the former group comparisons can be made with standard force constants for typical bonds.[40] Thus the force constant of C_1–C_2 elicits a bonding situation between single and double bonds, while C_2–C_3 looks like a typical triple bond. This latter conclusion must be qualified since self-consistent-field calculations overestimate the magnitude of force constants.[41,42] Furthermore, the method used to calculate them (force at two points) results only in a rough estimate of these quantities. Assuming a 20% error on the absolute value of the force constants one gets a bonding situation between double and triple bonds for the atoms C_2 and C_3. These numbers reflect the resonance structure picture of a typical alkynyl cation. The remaining force constants in the control space are significantly smaller than the bond stretching force constants. They correspond more to typical bendings. This is interesting since among them are the C_1–O_1 and C_3–O_2 stretchings, thereby indicating a weak interaction as it is required by the model in ref 1.

The variables used to define the control space can quite naturally be gathered into two subgroups: those changing significantly with the reaction progress and those that are much less affected. In the former subgroup of carbon–oxygen distances, the bending associated with the angles $\angle HC_3C_2$ (which characterize the hybridization change at C_3, $sp \rightarrow sp^2$) and $\angle O_1C_1C_2$ (hybridization change at C_1) are the most conspicuous. As is shown elsewhere[43] these four coordinates form the minimal control space necessary to yield the saddle point. Interestingly, the matrix element $\partial^2V/\partial R_1\partial R_2$ is not sufficient to produce a negative eigenvalue if the control space is reduced to the standard variables R_1 and R_2 whose second derivatives are positive. Rehybridization is essential in this context. It follows from these results that the control space can be further reduced if related compounds are to be calculated. This technique has been used to check upon the TS for the anti attack.

An invariant index as the geometry relaxes in the quadratic region toward the TS is the negative charge at the C_2 center. The second derivative of the energy as a function of the linear bending ($\angle C_1C_2C_3$) is remarkably constant. This index is intimately related to the reactivity of the alkynyl structure which has already been discussed.[44]

The activation energy obtained with the 4-21G basis set amounts to 5.7 kcal/mol, which is fairly similar to the MINDO/3 figure. These values are much lower than the activation parameters from ref 1. This point will be discussed later (cf. section V).

The ME profile for MINDO/3 produces a stepwise mechanism while 4-21G is a one-step asynchronic concerted process. An attempt to localize a possible intermediate in the 4-21G hypersurface to give a fair comparison with MINDO/3 has been made. The region found in a direction $R_1 + R_2$ has been explored (cf. Figure 6). At the saddle point this direction roughly coincides with the first and smaller positive eigenvalue (0.070) of the force constant ($\chi_\perp$ in Figure 6). It is associated with a symmetric fluctuation of the C_1–O_1 and C_3–O_2 distances together with angular variables numbers 5, 6, 7, and 8 of Table I. Along this direction one may come into a neighborhood of the points X_1 and X_2 in Figure 6. As pointed out before, the point X_1 is not stationary (note that this zone corresponds to the metastable structure on the MINDO/3 hypersurface). X_1 is about 18 kcal/mol above the TS. It is clear from this picture that the pathway will very unlikely be taking the direction indicated by MINDO/3 in the present hypersurface. The interesting result is X_2 which is a saddle point with two negative eigenvalues (saddle point of order two[45]). Pictorially speaking, this latter point is on a flat ridge and it is

(40) Wilson, E., Jr.; Decius, J. C.; Cross, P. C. *Molecular Vibrations*; Dover Publications, Inc.: New York, 1980.
(41) Fogarasi, G.; Pulay, P. *Annu. Rev. Phys. Chem.* **1984**, *35*, 191.
(42) Hess, B. A., Jr.; Schaad, L. J.; Carsky, P.; Zahradnik, R. *Chem. Rev.* **1986**, *86*, 709.
(43) Tapia, O.; Cardenas, R.; Andres, J., in preparation.
(44) (a) Andres, J.; Silla, E.; Bertran, J.; Tapia, O. *J. Mol. Struct. THEOCHEM* **1984**, *107*, 211. (b) Andres, J.; Cardenas, R.; Tapia, O. *J. Chem. Soc., Perkin Trans. 2* **1985**, 363.
(45) (a) Banerjee, A.; Adams, N.; Simons, J.; Shepard, R. *J. Phys. Chem.* **1985**, *89*, 52. (b) Heidrich, D.; Quapp, W. *Theor. Chim. Acta* **1986**, *70*, 89.

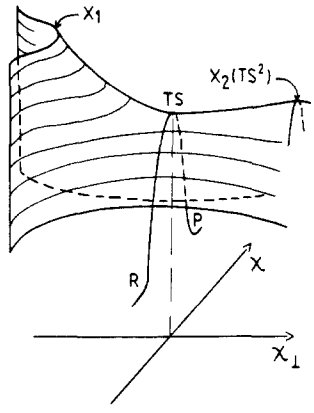

Figure 6. Schematic description of the saddle point region from 4-21G basis set calculation. $\chi_\perp$ is the perpendicular to the control coordinate at the saddle point. The direction along χ symbolizes the reaction path connecting the stationary points describing the reactant (R), transition state (TS) and product in the RLS model. All are stationary points on the global hypersurface. Total energies in atomic units for the reactant, saddle point, and product on the calculated ME profile are −344.373 806, −344.364 740, and −344.371 985, respectively. For the anti attack the energies of R, TS, and P are −344.372 356, −344.365 730, and −344.372 717, respectively. The geometries of R and P are given in order for each of the internal coordinates identified in Figure 5: C_1–C_2 = 1.440 and 1.300 Å; C_2–C_3 = 1.185 and 1.273 Å; C_3–H = 1.053 and 1.062 Å; C_3–O_2 = 3.014 and 1.586 Å; C_1–O_1 = 1.676 and 3.009 Å; O_2–H = 0.964 and 0.968 Å; O_1–H = 0.967 and 0.964 Å; C_1–C_{met} = 1.527 and 1.517 Å; C_{met}–H = 1.080 and 1.080 Å; $\angle C_1C_2C_3$ = 179.90° and 179.48°; $\angle$H–C_3–C_2 = 179.26° and 137.38°; $\angle O_1C_1C_2$ = 98.23° and 119.03°; $\angle O_2$–C_3–C_1 = 109.69° and 116.19°; $\angle$H–O_2–H = 106.72° and 115.76°; $\angle$H–O_1–H = 117.24° and 107.60°; $\angle C_{met}$–C_1–C_2 = 115.84° and 120.34°; $\angle$H–C_{met}–C_1 = 110.03° and 110.03°; dihedral angles $\angle$H–O_2–C_3–C_2 = 90.0° and 105.48°, $\angle C_{met}$–C_1–C_2–O_1 = 71.28° and 86.11°.

1.4 kcal/mol over the TS (cf. Figure 6). Structurally, X_2 is an alkynyl cation with two water molecules located at a distance of approximately 3.0 Å. One can see that the passage via an alkynyl cation is not at all forbidden, which is in good agreement with expectations concerning the role played by this type of carbocation in Rupe and Meyer–Schuster reactions.[1-3,20,21] From the Monte Carlo study[7] one can conjecture that the structure of the solvation shell around the TS will determine the issue. In particular the distribution of "holes" in the neighborhood of the ingoing and outgoing water molecules anticipates some aspect of solvent structure control on this reaction. This problem will be discussed in a forthcoming communication.[46]

V. Mechanism: Theory and Experiment

Although the geometry and electronic structure of transition states cannot be accurately measured by spectroscopic and diffraction techniques, kinetic data and isotope effects have been used to produce relatively accurate "robot portraits" of these structures. Bunton and Shiner have suggested that a distinction among appropriately chosen models for the TS of acid-catalyzed reactions can be made by using isotope effects in deuterium oxide solution.[47] Edens et al. used this method to portray the TS structure of the Meyer–Schuster reaction: see Model g in Chart I of ref 1.

The 4-21G TS structure depicted in Figure 5 corresponds now to a well-defined realization of Model g; and the trans configuration is the image of this Model g. The difference in R_1 and R_2 distances elicits the differences of the interactions between the corresponding centers. With use of ref 1 language, the model corresponds to nucleophilic attack, i.e., partial covalent attachment of H_2O at the C_3 terminus on a solvated ion. The degree of rearrangement at C_3 (rehybridization change sp → sp^2) can be measured by the change of the $\angle HC_3C_2$ (from 180° to a maximum change leading to 120°). For the 4-21G TS structure this is 24% of maximum. For (TS_1) MINDO/3 and TS (STO-3G) they are 27% and 53%, respectively. The experimental figure given for the compound with $R^1 = R^2 = C_6H_5$ is 34% of maximum.[1]

The degree of "covalent" attachment to C_3 depends on the stability of the alkynyl cation. This is elicited in a study of substituted compounds since the C_3–O_2 distance increases as the number of methyl groups decreases.[43] The correlation between the results on TS structures and the relative stability of the corresponding alkynyl cations[48] becomes apparent.

The activation free energy determined for a number of related compounds[1] shows important activation enthalpies (ca. 18 kcal/mol) and entropic effects. The experimental values refer to the unprotonated alcohols, thereby including the heat of reaction for alcohol protonation which is likely to be a positive quantity. The activation energy computed here does not contain the heat of protonation but elicits the intrinsic contribution of the water attack in the RLS. This barrier amounts to 5.7 kcal/mol. This theoretical barrier can increase due to (i) correlation effects and (ii) solvent effects. The first factor is expected to increase the activation energy; although hydroxyl group protonation produces an elongation of the C_1–O_1 bond length when compared to the parent alcohol[49] this is a covalent bond, while at the TS structure the distances between the carbon frame and the oxygen atoms correspond to an intermolecular electrostatic interaction. The correlation effects of the covalent bond are not compensated by the weak van der Waals interactions at the TS. An estimate for the correlation barrier can be obtained from a comparison with the hydride exchange reaction.[50] The correlation contribution to the activation barrier when one closed electronic shell group exchanges is ca. 3.5 kcal/mol, and in the present case we have two groups that may contribute with ca. 7 kcal/mol. As to the second factor, Monte Carlo simulations[7] show an increase in activation energy of about 6 kcal/mol. Taken together, the activation energy will be a figure of the order of 19 kcal/mol which moves the results in the right direction.

From the discussion above it is clear that only the 4-21G results are in accord with information derived from experiments. STO-3G differs in energy, while MINDO/3 yields a reasonable energy but a wrong pathway.

The first step of the mechanism can be represented as either specific or general acid catalysis. The data reported by Edens et al.[1] are not sufficient to discern among both. The minimal solvation model for the RLS includes the former, and it prepares the system to undergo the reaction. Thus, the calculated force constant of the C_1–O_1 bond is reduced from 5.1 to 1.6 (mdyn/Å) by protonation. The interatomic distance in this bond goes from 1.47 to 1.67 Å when protonation takes place. The effective charge at C_3 goes from −0.34 to −0.19 (au of charge). These results show that specific protonation is necessary to activate the alcohol. General acid catalysis is less effective in softening the C_1–O_1 bond as calculations with a second water molecule show (unpublished results). Since the reaction takes place in hyperacid media, the specific protonation model seems to be more adequate in describing the RLS in the MSM.

Until now, only the pathway representing the RLS has been discussed. The global hypersurface of the MSM contains more information as, for instance, the solvated structures in Figures 2 and 3 reveal. Let us now examine the topography of the 4-21G hypersurface.

This global hypersurface hints at one of the roles many-body solvent effects may be playing in the mechanism. The TS of the RLS separates two chemically different regions of the energy hypersurface: the protonated acetylenic alcohol from the protonated allenol. In each zone there are other stationary points corresponding to local solvation sites. For the reactant structure

(46) Tapia, O.; Lluch, J. M.; Cardenas, R.; Andres, J., in preparation.
(47) Bunton, C. A.; Shiner, V. J., Jr. *J. Am. Chem. Soc.* **1961**, *83*, 42, 3207, 3214.
(48) (a) Pittman, C. U., Jr.; Wilemon, G.; Fojtasek, J. E.; Kispert, L. D. *J. Phys. Chem.* **1975**, *79*, 2443. (b) Mirejovsky, D.; Drenth, W.; Van Duijneveldt, F. B. *J. Org. Chem.* **1978**, *43*, 763. (c) Dorado, M.; Mo, O.; Yañez, M. *J. Am. Chem. Soc.* **1980**, *102*, 947.
(49) Andres, J.; Silla, E.; Tapia, O. *J. Mol. Struct. THEOCHEM* **1983**, *105*, 307.
(50) Tapia, O.; Andres, J.; Aullo, J. M.; Bränden, C. I. *J. Chem. Phys.* **1985**, *83*, 4673.

there are at least two local solvation sites of relevance: the OH_2 group of the protonated alcohol and the ≡C—H carbo acid. These solvation sites are minima connected by a continuous pathway passing through the point characterizing the reactant in the RLS. This defines a solvation geodesic in contradistinction to the reactive pathway associated to the RLS. A similar situation is found for the product in the RLS (here the OH_2 group of the protonated allenol and the C–H carbo acid groups of the methyl are operational). Both at R and P the curvature along the solvation geodesic is negative. The region is however flat (the eigenvalues are −0.026 and −0.114 for the P and R, respectively). Of course, the curvature along the geodesic leading to the transition structure of the RLS studied above is positive, although rather flat (cf. Figure 6 and Table I). In vacuo, the RLS is represented in this model by a geodesic connecting three saddle points.[51]

The Meyer–Schuster rearrangement is a solvent-assisted reaction. The information contained in the in vacuo energy hypersurface has to be used in conjunction with actual representations of many-body solvation effects.[7] From the MC study reported in ref 7 it can be seen that the solvation sites are occupied by water molecules. Furthermore, the positions for syn and anti attack are not void.[46] Therefore, one may suspect the unstable structure for the reactant in vacuo becomes stabilized by many-body solvent effects. In other words, the cage solvent effect seems to be the way to prepare stable reactant for the rate-limiting step in this reaction. As the transition structure of the RLS correctly describes available physical chemistry information, one may conjecture that the transition state in solution must be poorly solvated.[46]

An important result concerning the mechanism of the Meyer–Schuster reaction derives from the present and companion studies on the intramolecular model.[4,5] A unifying feature of the reaction pathways emerges, namely, the presence of a (slightly deformed) alkynyl cation interacting electrostatically with one (intramolecular) or two (intermolecular) water molecules. The TS (saddle point) arises from the interactions between water and the C_1 and C_3 centers in the alkynyl cation. Notice that the results are similar if the 4-31G instead of 4-21G basis set is used. The fact that this cation can be detected in non-aqueous acid media by solvolysis of tertiary acetylenic alcohols and not that easily in aqueous acid media[6] can naturally be rationalized by studying fluctuations along the $R_1 + R_2$ direction. In aqueous media, the carbocation may be entering the Rupe reaction, and the probability of finding it as a transient is smaller than in non-aqueous media. Interestingly, these alkynyl carbocations have been used to explain the mechanism of this kind of reaction.[1-3,20,21] The theoretical results suggest that it is the nature of the solvent which will determine the structure of the transition state as well as the appearance of an intermediate alkynyl cation for this reaction.

The question raised by Jencks[52] on whether carbocations are intermediates or transition states in the present case can be answered as follows: they can have both qualities. The alkynyl cation is part of a saddle point structure in the minimal solvation model, and if one realizes that this species is in water, the solvent will produce short-lived cages[7,13] that stabilize, by inertial effects, the intrinsically unstable species. It is not difficult to conclude that the driving force for both the Meyer–Schuster and Rupe rearrangements appears to be the irreversible process leading to the formation of unsaturated carbonyl compounds from the "intermediate" carbonium ions.

VI. Discussion

An extensive theoretical study employing analytical first derivatives and numerical second derivatives of the total energy with respect to internal coordinates of the rate-limiting step for the 1,3-hydroxyl shift in tertiary propargyl alcohols has been presented. Semiempirical and ab initio MO methods have been used to determine minimum-energy profiles and to characterize the stationary points on the corresponding energy hypersurfaces. Minimal and double-ζ quality basis sets have been used. The results have been contrasted with mechanistic information derived from solvent isotope effects and kinetic measurements. A satisfactory description of the reaction step is obtained from a 4-21G basis set level only. CNDO/2 gives a nonsense description, STO-3G only describes the presence of an activation barrier, while MINDO/3 gives a two-step description via an intermediate state.

There are problems not yet solved concerning the validity of semiempirical and approximate MO reactive minimum energy profiles. All procedures that are based on a one-determinant Hartree–Fock method do not adequately represent homolytic bond breaking and forming processes. The reaction studied here involves a concerted bond breaking and forming where the exiting and entering groups are closed shell species (water) and, in principle, one is not confronted with the usual shortcomings of the HF SCF schemes.

For a number of reactions where a comparison between ab initio and approximate MO outcomes can be made, it is observed that the presumed transition states differ in nature.[16] For example, discrepancies have been found for the TS structure in the Diels–Alder reaction: ab initio calculations predict a synchronous mechanism,[53,54] while MINDO/3 calculations show an asynchronous one;[55-58] the transition state structure being clearly asymmetric in the latter case. These issues have recently been discussed by Dewar et al.[59] where MINDO/3 and MNDO calculations are compared to different basis set results. Bernardi et al.,[60] however, show the inadequacy of the previous calculation by using ab initio 4-31G and CI calculations. There is also controversy concerning the mechanism of the 1,3-dipolar cycloadditions. Again, ab initio predicts a synchronous and MINDO/3 and MNDO[61,62] predict an asynchronous mechanism. Moreover, in some cases the index of the stationary point associated with the presumed TS geometry differs: for the isomerization of methyl isocyanide to methyl cyanide (acetonitrile), MINDO/3 yields a minimum[63] while ab initio calculations lead to an index of 1 (saddle point).[64] A similar situation is found for hydride transfer reactions.[50,65] The MINDO/3 ME profile shows a metastable state where double-ζ wave functions display a saddle point.[50] In the absence of experimentally based information of the TS structure, of course, it is nearly impossible to settle the controversy. Recently, experimental evidence for the concerted mechanism of the Diels–Alder reaction of butadiene with ethylene has been reported by Houk et al.[66]

(51) This feature is nearly impossible to find for the CNDO/2 and STO-3G methods since in this region the hypersurface is flat. For the STO-3G hypersurface the negative eigenvalue for the reactant is −0.05. Furthermore, the constraint used to perform the calculations hides the negative curvature. In the 4-21G case a walk down from the TS was done and the force constant matrix diagonalized at the attained stationary points. A similar procedure was followed to get down to the solvation sites. Thus, on the hypersurface there must be a continuous pathway connecting the stationary points that at the saddle point has the tangent coinciding with the direction of the eigenvector associated to the unique negative eigenvalue. It is in this sense that the term geodesic is used in this discussion. Interestingly, the curvature associated with the angular displacement of the ingoing water molecule changes sign when the system moves from the R along the reactive geodesic that connects to P via the TS in the RLS representation. This degree of freedom controls the displacement along the solvation geodesic.

(52) Jencks, W. P. *Acc. Chem. Res.* **1980**, *13*, 161.

(53) (a) Burke, L. A.; Leroy, G.; Sana, M. *Theor. Chim. Acta* **1975**, *40*, 313. (b) Burke, L. A.; Leroy, G. *Theor. Chim. Acta* **1977**, *44*, 219.
(54) Townsend, R. E.; Ramuni, G.; Segal, G.; Hehre, W. J.; Salem, L. *J. Am. Chem. Soc.* **1976**, *98*, 2190.
(55) Jug, K.; Kruger, H. W. *Theor. Chim. Acta* **1979**, *52*, 19.
(56) Dewar, M. J. S.; Griffin, A. C.; Kirschner, S. *J. Am. Chem. Soc.* **1974**, *96*, 6225.
(57) Dewar, M. J. S.; Olivella, S.; Rzepa, H. S. *J. Am. Chem. Soc.* **1978**, *100*, 5650.
(58) Oliva, A.; Fernandez-Alonso, J. I.; Bertran, J. *Tetrahedron* **1978**, *34*, 2029.
(59) Dewar, M. J. S.; Olivella, S.; Stewart, J. J. P. *J. Am. Chem. Soc.* **1986**, *108*, 577.
(60) Bernardi, F.; Bottoni, A.; Robb, M. A.; Field, M. J.; Hillier, I. H.; Guest, M. F. *J. Chem. Soc., Chem. Commun.* **1985**, 1051.
(61) (a) Poppinger, D. *J. Am. Chem. Soc.* **1976**, *98*, 7486. (b) Poppinger, D. *Aust. J. Chem.* **1976**, *29*, 465.
(62) Dewar, M. J. S.; Pierini, A. *J. Am. Chem. Soc.* **1984**, *106*, 203.
(63) Dewar, M. J. S.; Kohn, M. C. *J. Am. Chem. Soc.* **1972**, *94*, 2705.
(64) (a) Liskow, D. H.; Bender, C. F.; Schaefer, H. F., III *J. Chem. Phys.* **1972**, *57*, 4509. (b) Redmon, L. T.; Purvis, G. D.; Bartlett, R. J. *J. Chem. Phys.* **1978**, *69*, 5386.
(65) Donkersloot, M. C. A.; Buck, H. M. *J. Am. Chem. Soc.* **1981**, *103*, 6549.

These results disclaim an asynchronous stepwise mechanism as predicted from the MINDO/3 calculations. In the present study the exploration of the relevant sections of the 4-21G hypersurface and the experimentally based information of the TS properties suggest that the MINDO/3 profile might be a numerical artifact.[67]

The STO-3G model produces poor descriptions of reaction profiles of the S_N2[68] and hydride exchange reactions.[50] In the present case, and in spite of the presence of a cationic species all along the pathway, the STO-3G model is again unsatisfactory. Therefore, STO-3G ME profiles for predicting the nature of the species along a reaction must be taken with circumspection.

The Meyer–Schuster rearrangement is a solvent-assisted reaction. The MSM is a first step toward representing solvent effects in the supermolecule approach. Even at this simple level the global hypersurface hints some of the roles passive many-body solvent effects might have on this reaction. Metropolis Monte Carlo simulations of hydration effects on the stationary points of the present reaction[7] have shown interesting solvation patterns. Solvent caging effects may play an important role in stabilizing the reactant and product of the RLS. Furthermore, if the solvation shell around the TS is allowed to equilibrate, the sample analysis shows the presence of two water molecules interacting with the C_2 center.[7] As we have seen before, increment in the number of water molecules has produced a change in the structure of the TS. The question arises, naturally, as to what may happen to the TS structure if another water molecule is added to the MSM and the system is treated as a new supermolecule. The present results obtained with the MSM are in fairly good agreement with available physical organic chemistry information. Therefore, one would not expect a departure from the simple molecular model used here.[46]

Acknowledgment. The computations have demanded huge amounts of CPU time over the recent years. We are most grateful to Uppsala Data Center for facilities made available in the CYBER 170-835 and IBM-Sweden for extensive use of the 4361 computer thanks to a Study Contract with the Molecular Biology Department. We thank the Immunology Department at BMC for letting us use their MICRO VAX-II without constraints. J.A. acknowledges a post-doctoral fellowship (curso 84/85) from the Spanish Government (Ministerio de Educacion y Ciencia) to carry out this research at the Chemistry and Molecular Biology Department, BMC. O.T. acknowledges financial support from the Swedish Research Council.

(66) Houk, K. N.; Lin, Y. T.; Brown, F. K. *J. Am. Chem. Soc.* **1986**, *108*, 554.
(67) The geometrical parameters for the stationary points with the 4-21G basis set have been given in the captions for Figures 5 and 6. These data can be used to check semiempirical methods in this type of study.
(68) Kost, D.; Aviram, K. *J. Am. Chem. Soc.* **1986**, *108*, 2006.
(69) (a) Zielinski, T. J.; Breem, D. L.; Rein, R. *J. Am. Chem. Soc.* **1978**, *100*, 6266. (b) Klopman, G.; Andreozzi, P.; Hopfinger, A. J.; Kikuchi, O.; Dewar, M. J. S. *J. Am. Chem. Soc.* **1978**, *100*, 6267.
(70) (a) McIver, J. W., Jr.; Stanton, R. E. *J. Am. Chem. Soc.* **1972**, *94*, 8618. (b) Stanton, R. E.; McIver, J. W., Jr. *J. Am. Chem. Soc.* **1974**, *96*, 3632.
(71) (a) Murrell, J. N.; Laidler, K. J. *Trans. Faraday Soc.* **1968**, *64*, 371. (b) Murrell, J. N.; Pratt, G. L. *Trans. Faraday Soc.* **1970**, *66*, 1680. (c) Murrell, J. N. *J. Chem. Soc., Chem. Commun.* **1972**, 1044.

Two-Dimensional Double-Quantum NMR Spectroscopy of Isolated Spin $^3/_2$ Systems: ^{23}Na Examples†

William D. Rooney, Thomas M. Barbara, and Charles S. Springer, Jr.*

Contribution from the Department of Chemistry, State University of New York, Stony Brook, New York 11794-3400. *Received April 6, 1987*

Abstract: Of the four possible types of NMR spectral behavior for a system consisting of isolated quadrupolar $I = {}^3/_2$ nuclei, double-quantum coherence can be excited by multipulse techniques in three. Two-dimensional ^{23}Na NMR spectra have been obtained from samples exhibiting each of these three. These are the following: (a) single crystal (represented here by an oriented lyotropic liquid crystal), (b) powder pattern (represented by an unoriented lyotropic liquid crystal), and (c) homogeneous biexponential relaxation (represented by a sufficiently dense solution of reasonably globular macromolecules). The fourth type, for which double quantum coherence generation by pulsed NMR is unknown, is the extreme narrowed situation. The pulse sequence $(90_x\text{-}\tau/2\text{-}180_y\text{-}\tau/2\text{-}90_x\text{-}t_1\text{-}90_x\text{-}t_2)$ generates a two-dimensional spectrum when the response is sequentially Fourier transformed from the t_2 and t_1 time domains. The projection onto ν_2 is the single-quantum spectrum while the projection onto ν_1 is the double-quantum spectrum (given appropriate phase cycling of the pulse sequence). The double-quantum spectrum is quite distinct for all three spectral types. This is also true for the single-quantum spectrum. However, the latter is less diagnostic and is subject to distortions from an insufficiently short receiver dead time, while the former is not. In addition, all of the double-quantum spectral information derives from modulation of the strong, sharp central single-quantum signal. Thus, this experiment can be useful in cases where the broad satellite resonance(s) is (are) not detectable in the single-quantum spectrum because of electric field gradient effects on the quadrupolar nucleus. This is often the case in tissue-containing samples. The theory of this experiment is briefly discussed, as are the differing requirements for the excitation of double quantum coherence for type a and type b spectra on the one hand and type c spectra on the other. Drawbacks of this approach, particularly the trade-off between total acquisition time and digital resolution in the ν_1 dimension, are also considered.

In conventional single quantum (1Q) NMR spectroscopy and imaging, adjacent states established by the Zeeman interaction are brought into coherent superposition by the absorption or emission of a radio frequency photon. The 1Q NMR spectra of nuclei with electric quadrupole moments ($I \geq 1$, where I is the nuclear spin quantum number) are often strongly affected by interactions with electric field gradients (EFG). Potentially, these interactions contain a wealth of information about the system under study. Unfortunately, they are often difficult (sometimes impossible) to measure in the standard 1Q NMR experiment. Important examples of this arise in the ^{23}Na and ^{39}K (both $I = {}^3/_2$ nuclei) spectra from living systems.[1] These are isotopes of

† Presented in part, at the March Meeting of the American Physical Society, New York, NY, March, 18, 1987 (abstract: *Bull. Am. Phys. Soc.* **1987**, *32*, 644) and the 28th Experimental Nuclear Magnetic Resonance Spectroscopy Conference, Asilomar, CA, April, 5, 1987.

(1) Springer, C. S. *Annu. Rev. Biophys. Biophys. Chem.* **1987**, *16*, 375-399.

0002-7863/88/1510-0674$01.50/0